Electrochimica Acta 398 (2021) 139298

Contents lists available at ScienceDirect

Electrochimica Acta

journal homepage: www.elsevier.com/locate/electacta

Synthesis of selenophene substituted benzodithiophene and fluorinated benzothiadiazole based conjugated polymers for organic solar cell applications

Sultan Taskaya Aslan[a], Duygu Cevher[b], Eda Bolayır[a], Gonul Hizalan Ozsoy[c], Yasemin Arslan Udum[d], Erol Yıldırım[a,b,f], Levent Toppare[a,b,c,e], Ali Cirpan[a,b,c,f,*]

[a] Department of Chemistry, Middle East Technical University, 06800, Ankara, Turkey
[b] Department of Polymer Science and Technology, Middle East Technical University, 06800, Ankara, Turkey
[c] ODTU GUNAM, Middle East Technical University, Ankara, 06800, Turkey
[d] Technical Sciences Vocational High School, Gazi University, 06374, Turkey
[e] Department of Biotechnology, Middle East Technical University, Ankara, 06800, Turkey
[f] Department of Micro and Nanotechnology, Middle East Technical University, 06800, Ankara, Turkey

ARTICLE INFO

Article history:
Received 5 August 2021
Revised 15 September 2021
Accepted 19 September 2021
Available online 28 September 2021

Keywords:
Benzodithiophene
Benzothiadiazole
Fluorine substitution
Power conversion efficiency
Organic solar cell

ABSTRACT

A series of alternating conjugated copolymers which contain selenophene modified benzodithiophene and fluorine bearing benzothiadiazole have been synthesized via Stille polycondensation reaction to investigate the effect of the number of fluorine atoms substituted to the benzothiadiazole. Three different polymers, **PBDTSe-BT, PBDTSe-FBT** and **PBDTSe-FFBT**, were reported and their electrochemical, spectroelectrochemical, and photovoltaic behaviors were examined. Density functional theory calculations were performed on model tetramer structures to shed light on how substituting the fluorine atom to the acceptor building block affects the structural, electronic and optical properties of the polymers. The results of computational studies were compared with experimental studies. The structure adjustment accomplished by fluorine substitution on the benzothiadiazole moiety reveals an influence on the electronic structure of polymers with a more negative HOMO energy level. A high V_{OC} for the resulting photovoltaic device was examined for **PBDTSe-FFBT**. Difluorinated polymer **PBDTSe-FFBT**:$PC_{71}BM$ organic solar cell exhibited the highest photovoltaic performance of 2.63% with J_{SC} of 7.24 mA cm^{-2}, V_{OC} of 0.72 V and FF of 50.6%. **PBDTSe-BT**:$PC_{71}BM$ revealed the best PCE as 2.39%, and the device reached the highest efficiency up to 1.68% for **PBDTSe-FBT**:$PC_{71}BM$.

1. Introduction

Producing renewable energy to obtain electricity from sunlight via photovoltaic devices is a global issue. Inorganic or perovskite solar cell devices harvest solar energy efficiently; however, these conventional devices are not economically feasible compared to organic solar cells. This is the major reason for the improvement of organic photovoltaic (OPV) materials and devices. [1] Due to the low-cost, roll-to-roll production of flexible, large-area, light weight photovoltaic devices, organic bulk heterojunction (BHJ) solar cell devices incorporating conjugated polymers have drawn notable attention from both industrial and academic communities during the past decades. [2–6]

The search continues for the performance of the BHJ solar cells to obtain high power conversion efficiencies (PCEs). The properties of conjugated polymers as an active layer for organic photovoltaic applications are the most determinant factor to improve the PCE. Therefore, a broad solar absorption with high absorption coefficient to ensure harvesting the solar light effectively and a high charge carrier mobility for charge transport are required for enhancement of the PCE. [7] Moreover, a large energy balance between the highest occupied molecular orbital (HOMO) of the donor material and the lowest unoccupied molecular orbital (LUMO) of the acceptor material is necessary to maximize the open-circuit voltage (V_{oc}). [8] A low band gap conjugated polymer donor material to increase the short-circuit current density (J_{sc}) and a sufficient degree of phase separation between the donor and acceptor domains inside the photoactive layer to enhance J_{sc} and the fill factor (FF) are also crucial for the improvement of the PCE of organic solar cells. [1,9,10]

* Corresponding author.
E-mail address: acirpan@metu.edu.tr (A. Cirpan).

https://doi.org/10.1016/j.electacta.2021.139298
0013-4686/

Several conjugated polymers involving electron donor and acceptor units in their main chain backbone or two-dimensional configurations (2-D) have been designed to tune the energy levels and harvest more photons from the solar light. Recently, several studies have been reported with high PCE reaching beyond 18% as a result of developing novel polymeric materials and device architectures. [5,11–14] In this regard, benzo[1,2-*b*:4,5-*b′*]dithiophene moiety was used as an electron donor with alkylselenophene side chain as an alternative to the thiophene. [15,16] As reported in the literature, lower aromaticity of selenophene with respect to the thiophene results in an improvement in the quinoid character of the polymer, which leads to lower band-gap energy, increased effective conjugation length and enhanced planarity. [17,18] Selenophene-based materials have also improved conductivity and charge mobility due to larger π-overlap leading to the greater π-orbitals of Se atoms and intermolecular Se-Se interactions. [19,20] Moreover, the Se atom has a much larger size and less electronegativity than the chalcogenophene homolog of the S atom; as a result, Se comprising polymers are more efficient at broadening the absorption spectrum near the infrared region. [21,22] Jiang et al. studied a series of polymers by changing S-atoms with Se-atoms on the side chains of the donor moiety, the acceptor units, and the π-bridge to examine the effect of Se-atom substitution and they reported a maximum PCE of 3.3% for PBDTTTBS containing thiophene substituted BDT and 4.0% for PBDTSTBS containing Se substituted BDT moiety. [22] Moreover, Byun et al. investigated the effect of substitution of dodecylselenophene side chain on BDT and reported 2.73% of maximum PCE. [23] Therefore, there is a need to work on the novel selenophene substituted BDT based polymers.

Recent studies have indicated that fluorination of the backbone of conjugated copolymers has been established to construct high-performance BHJ solar cell devices. [24,25] Because of the strong electron-withdrawing property, incorporating fluorine atoms into D-A conjugated polymers results in lower HOMO energy levels leading to an increased V_{OC}. Moreover, the non-covalent interaction of fluorine atoms with the adjacent atoms (F···H/S/F/N) can cause strong π-π interactions which may induce fine-tuning of its morphology with fullerene. This interaction also may increase the charge mobility and the crystallinity of the active layer resulting in higher J_{SC} and FF. [26–31]

In the present study, 4,8-bis(5-(2-ethylhexyl)selenophen-2-yl)benzo[1,2-*b*:4,5-*b*']dithiophene (BDT-Se) was used as the donor unit and 4,7-bis(5–bromo-4-hexylthiophen-2-yl)benzo[c][1,2,5]thiadiazole was selected as the acceptor unit in an investigation of the effects of the fluorine substitution on the benzothiadiazole acceptor moiety. According to the literature, incorporating thiophene or other heteroaromatic rings into the D-A polymers can greatly affect the optoelectronic and photovoltaic properties of the organic solar cells (OSCs). [2,32,33] In this work, three conjugated polymers based on selenophene substituted BDT and benzothiadiazole building blocks were synthesized and used in OSCs. The structures of the resulting polymers referred to as **PBDTSe-BT, PBDTSe-FBT**, and **PBDTSe-FFBT**, are shown in Scheme 3. The n-hexylthiophene unit was introduced to the polymer backbone as π-bridges to improve the solubility and photovoltaic performance of benzothiadiazole-based polymers. Fluorine atoms were included in the benzothiadiazole structure as shown in Scheme 2. The effect of the number of fluorine atoms on electrochemical, spectroelectrochemical, and photovoltaic properties of the novel polymers was inspected thoroughly. The change in the morphology of blends with polymers and PCBM was also discussed in this study. The polymer **PBDTSe-FFBT** showed the most negative HOMO level between this series of polymers and the photovoltaic device based on **PBDTSe-FFBT**:$PC_{71}BM$ exhibited a V_{OC} of 0.72 V and a PCE of 2.63%.

2. Experimental

2.1. Materials

The starting materials and all reagents were purchased from commercial sources and used without further purification unless stated otherwise. The solvents used during the experiments were dried over common standard methods when needed. All reactions were performed under a nitrogen atmosphere unless otherwise noted. Column chromatography was carried out with Merck Silica Gel 60 (particle size: 0.063–0.200 mm, 70–230 mesh ASTM) as the stationary phase with different solvent systems for the purification of crude materials.

2.2. Instrumentation

Thermal properties were determined by a thermal gravimetric analyzer (Perkin Elmer Pyris 1 Thermogravimetric Analysis(TGA)) and Perkin Elmer Diamond Differential Scanning Calorimeter (DSC) with a heating rate of 10 °C/min under N_2. ^{1}H and ^{13}C Nuclear Magnetic Resonance Spectra were obtained via Bruker Spectrospin Avance DPX-400 Spectrometer with regard to trimethylsilane (TMS) as an internal reference. Gel permeation chromatography (GPC) technique (polystyrene as the Standard-Universal Calibration method) was used to determine the average molecular weights of the synthesized polymers **PBDTSe-BT, PBDTSe-FBT** and **PBDTSe-FFBT** in THF via Malvern-OmniSEC. In order to accomplish the spectroelectrochemical studies of **PBDTSe-BT, PBDTSe-FBT** and **PBDTSe-FFBT**, Varian Cary 5000 UV–Vis Spectrometer was used at ambient temperature. Gamry 600 potentiostat was used with a three-electrode consisting of a platinum wire, Ag wire, and Indium Tin Oxide (ITO)-coated glass configuration in 0.1 M tetra-butylammonium hexafluorophosphate/acetonitrile ($TBAPF_6$/ACN) electrolyte/solvent couple at 100 mV/s scan rate to achieve cyclic voltammetry studies of these polymers.

2.3. Synthesis of polymers

Synthesis of PBDTSe-BT

Compound **3** (0.15 g, 0.15 mmol) and compound **7** (94 mg, 0.15 mmol) were dissolved with 15 mL of toluene and 40 min of argon gas passed and $PdCl_2(PPh_3)_2$ (5.3 mg, 7.5 µmol) catalyst was added. The reaction mixture was heated to reflux and stirred for 42 h. Tributyl (thiophen-2-yl) stannane (0.118 g, 0.3 mmol) was added and stirred for a further 4 h, followed by the addition of 2–bromo thiophene (0.05 g, 0.3 mmol) for 4 h. The reaction mixture was then brought to room temperature and the polymer was precipitated by the addition of 50 mL of methanol. The precipitate was then extracted with Soxhlet with methanol, hexane, and chloroform. The polymer in the chloroform fraction was recovered as a purple solid by precipitation from methanol. The solid was dried under vacuum (120 mg, 70%). ^{1}H NMR (400 MHz, $CDCl_3$) δ 8.21 – 6.45 (Aromatic H), 2.95 (-CH_2), 1.88 – 0.61 (-CH_2, -CH_3).

Synthesis of PBDTSe-FBT

The same procedure was performed for **PBDTSe-FBT** using compound **3** (0.15 g, 0.15 mmol) and compound **11** (97 mg, 0.15 mmol) and the purple polymer was obtained from chloroform fraction (126 mg, 72%). ^{1}H NMR (400 MHz, $CDCl_3$) δ 8.28 – 6.38 (Aromatic H), 2.96 (-CH_2), 1.98 – 0.66 (-CH_2, -CH_3).

Synthesis of PBDTSe-FFBT

The same procedure was performed for **PBDTSe-FFBT** using compound **3** (0.15 g, 0.15 mmol) and compound **15** (0.1 g,

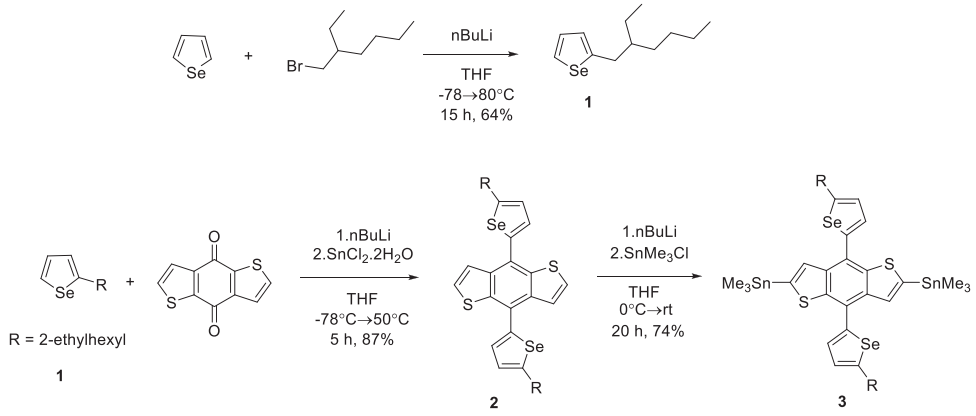

Scheme 1. Synthetic pathway of donor monomer.

0.15 mmol) and the purple polymer was obtained from chlorobenzene fraction (70 mg, 39%).

2.4. Computational Methods

Density functional theory (DFT) calculations were conducted for **PBDTSe-BT, PBDTSe-FBT** and **PBDTSe-FFBT** using tight convergence criteria in Gaussian09.Rev. A.02 software package at the B3LYP hybrid functional and 6–311G(d) basis set level, similar to the recent studies that have concordant results with the experimental studies. [34–41] Calculations were performed on model tetramer structures with four donors, four acceptors and eight bridge structures. Hexyl side chains on the thiophene bridges and 2-ethylhexyl units on donor were replaced with methyl groups in calculations not to exceed our computational capacity. Geometry optimizations were started from different initial conformations by altering the dihedral angle between consecutive repeating donor, acceptor and bridging units. Electrostatic potential surface (ESP), first three highest occupied molecular orbitals (HOMO, HOMO-1, HOMO-2), and three lowest unoccupied molecular orbitals (LUMO, LUMO+1, LUMO+2) were mapped onto the optimized model structures. Direct band gap (E_g) was calculated calculation of energy difference between the HOMO and LUMO for the optimized ground state, and the optical E_g^{opt} was determined by the $S_0 \rightarrow S_1$ transition, the first vertical excitation energy of the singlet excited state obtained by time-dependent density-functional theory (TDDFT). Vertical ionization potential (VIP) and vertical electron affinity (VEA) in addition to the adiabatic ionization potential (AIP), and adiabatic electron affinity (AEA) were also calculated by considering the transition from the neutral ground state to the charged structures at the ground state geometry and optimized charged geometries for cation and anions, respectively. Hole reorganization energies (λ_{reorg}) were determined based on Bredas et al. [42] formulation. The total atomic charges (δ) on the acceptor units based on the ESP fitting method of Merz-Kollman (MK)[43], dipole moment (μ), isotropic dipole (α) polarizability, anisotropy ($\Delta\alpha$) of the polarizability and first order hyperpolarizability (β) were calculated to elucidate experimental observations.

2.5. Fabrication of photovoltaic devices

Organic solar cell parameters for the **PBDTSe-BT, PBDTSe-FBT**, and **PBDTSe-FFBT** were investigated with the device structure of ITO/PEDOT:PSS/Polymer:$PC_{71}BM$/LiF/Al. The construction of the BHJ solar cell device was as follows; etching and cleaning of ITO, coating of the PEDOT:PSS, coating of the active layer and evaporating the metal. ITO coated glass substrates purchased from Visiontek were etched using an acid solution. The substrates were sonicated in an ultrasonic bath, respectively, using toluene, detergent (Hellmanex), water and isopropyl alcohol for 15 min. The substrates were dried with an N_2 gun after that O_2 plasma treatment was used to enhance the work function of ITO via removing organic impurities as well as to reduce the surface tension of ITO. PEDOT:PSS was filtered through a 0.45 µm PES syringe filter and coated on the ITO surface. Subsequently, the substrates were annealed at 135 °C for 15 min on the hot plate to evaporate the residual water. Polymer:$PC_{71}BM$ mixtures were prepared with different weight ratios, concentrations and additives, filtered through a 0.22 µm pore-sized PTFE syringe filter and coated on a PEDOT:PSS layer in the nitrogen-filled glove box. Lastly, the devices were completed by thermal evaporation of LiF and Al metal in a vacuum evaporation chamber on the Polymer:$PC_{71}BM$ layer. After the device construction, the current density voltage characteristics were tested using the Keithley 2400 under the Atlas Material Testing Solutions solar simulator (AM 1.5 G).

3. Results and discussion

3.1. Synthesis and characterization

The structure of the polymer and the structures of the modified donor and acceptor units required for their synthesis are given below (Scheme 3). All the intermediates and monomers were synthesized according to the given references. In our synthetic design, 2-ethylhexylselenophene substituted benzodithiophene and fluorinated benzothiadiazole derivatives were taken as the donor and acceptor units, respectively. The synthetic route for the donor compound is given in Scheme 1. Commercially available selenophene was reacted with commercial 2-ethylhexylbromide in the presence of *n*–butyl lithium to obtain compound 1. After that, the synthesis of compound **2** was achieved in high yield by the reaction of benzo[1,2-*b*:4,5-*b*′]dithiophene-4,8–dione with lithium derivative of compound **1** [44] followed by reduction of the corresponding diol with stannous chloride dihydrate in hydrochloric acid solution. The lithiation of compound **2** with *n*-buthyl lithium followed by quenching the lithium derivative with trimethyltin chloride resulted in the monomer compound **3** successfully. [44]

The detailed synthetic routes followed for the acceptor units **7, 11**, and **15** are given in Scheme 2. Compound **4** [45] and Compound **5** [46] were synthesized according to previously reported procedures. The Stille cross-coupling reaction between compound **4** and compound **5** afforded compound **6** [38], which was treated with N-bromosuccinimide to yield compound **7** [47]. The diamine derivatives of mono fluorinated and difluorinated benzene were purchased commercially. The ring closure reactions were performed

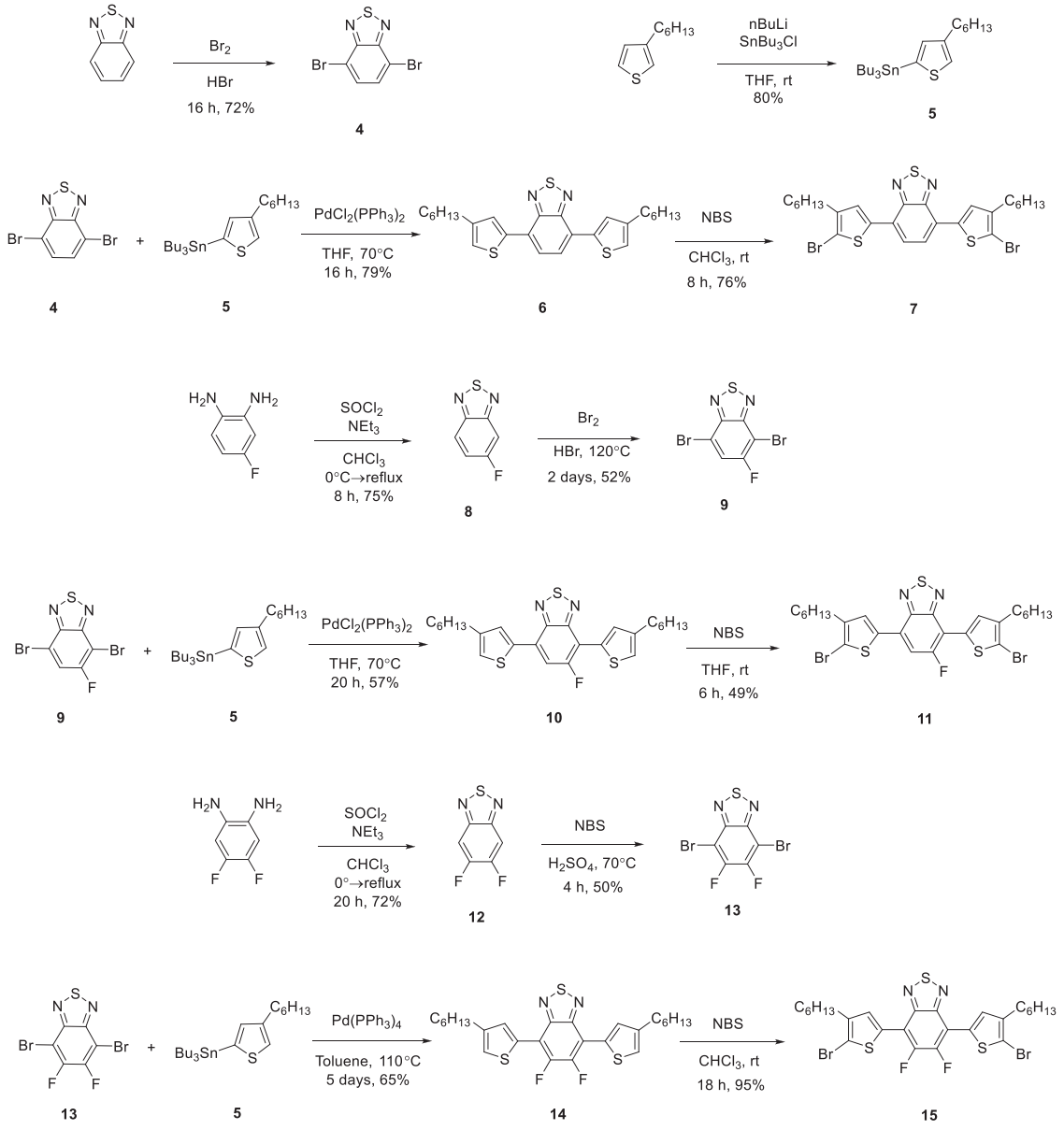

Scheme 2. Synthetic pathway of acceptor monomers.

with thionyl chloride to obtain **8** and **12**. The halogenation reactions were performed according to the procedures reported in the literature. [46,48] The treatment of compounds **9** and **13** [49] with tributyl (thiophen-2-yl)stannane (**5**) under Stille coupling reaction conditions produced the target molecules **10** and **14** which were brominated with N-bromosuccinimide to yield target monomers **11** and **15**. [49,50] Further synthetic details are given in Supporting Information.

The routes for the synthesis of three polymers are shown in Scheme 3. **PBDTSe-BT, PBDTSe-FBT** and **PBDTSe-FFBT** were prepared via typical Stille cross-coupling reaction between organotin monomer of BDT (**3**) and bromothiophene flanked benzothiadiazole derivatives (**7, 11** and **15**) using tetrahydrofuran as solvent and bis(triphenylphosphine)palladium(II) dichloride ($PdCl_2(PPh_3)_2$) as the catalyst. The gel permeation chromatography (GPC), which measured the molecular weights and polydispersity index (PDI) of the three polymers are displayed in Table 1. All polymers show good solubility in chloroform, chlorobenzene (CB) and other common solvents, which are favorable for film fabrication.

Table 1
Summary of GPC and TGA studies.

	Mn/kDa	Mw/kDa	PDI	T_d*/ °C
PBDTSe-BT	8.7	29.6	3.4	443
PBDTSe-FBT	10.1	29.7	2.9	437
PBDTSe-FFBT	13.5	91.7	6.8	400

* corresponding to 5% weight loss in the thermogravimetric analysis

3.2. Thermal studies

Differential scanning calorimetry (DSC) and thermogravimetric analysis (TGA) were utilized to determine the thermal properties of the polymers. **PBDTSe-BT, PBDTSe-FBT** and **PBDTSe-FFBT** have good thermal stability with degradation temperatures over 400 °C, which are sufficient for the application in an organic solar cell. The TGA measurements showed that 5% weight loss degradation temperatures (T_d) of **PBDTSe-BT, PBDTSe-FBT** and **PBDTSe-FFBT** were

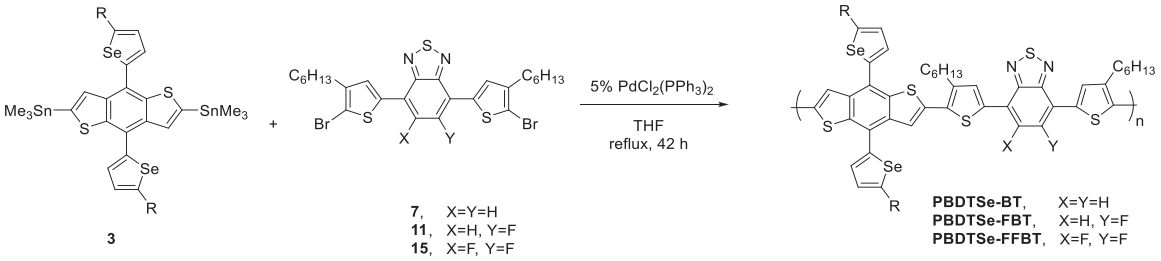

Scheme 3. Synthetic pathway of polymers.

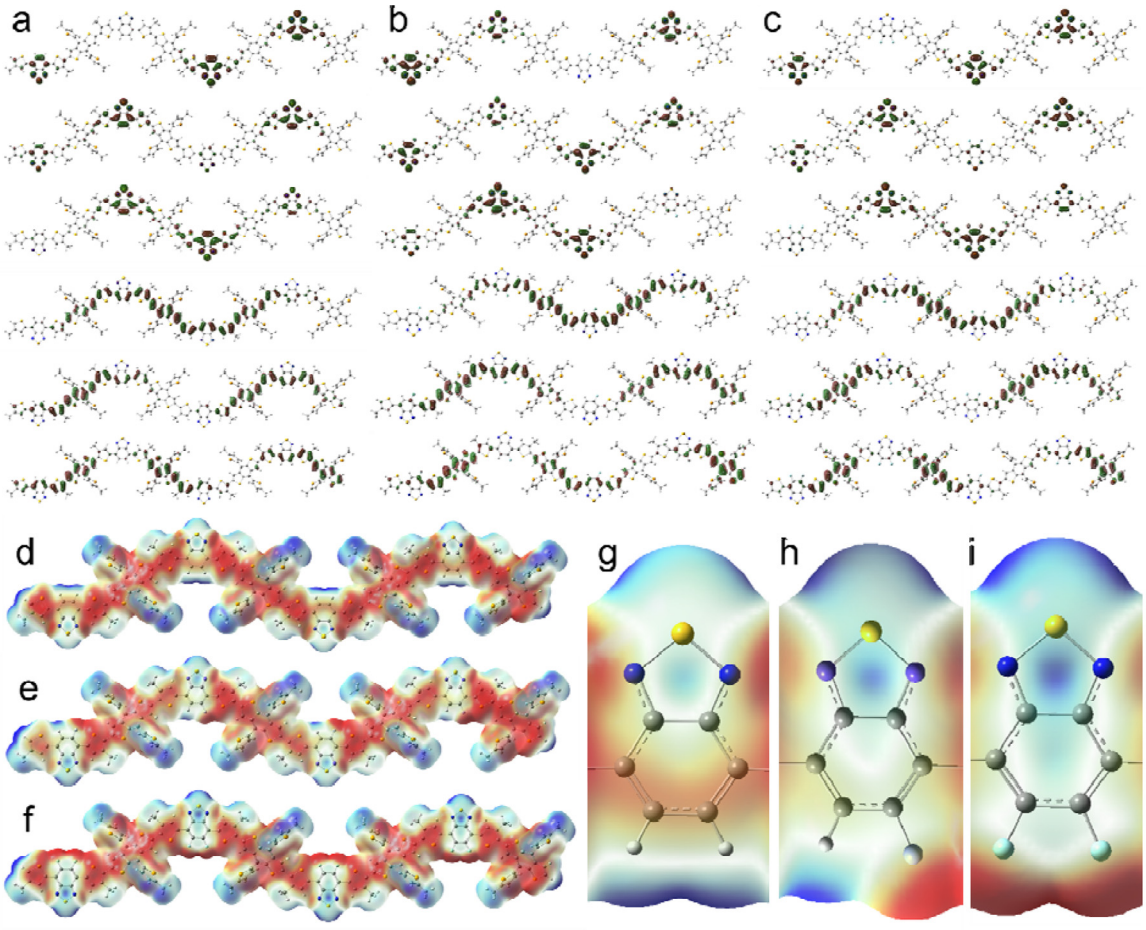

Fig. 1. Frontier molecular orbital surfaces (from top to down: LUMO+2, LUMO+1, LUMO, HOMO, HOMO-1, HOMO-2) for a) **PBDTSe-BT**, b) **PBDTSe-FBT**, c) **PBDTSe-FFBT** and electrostatic potential surface (ESP) for the d) **PBDTSe-BT**, e) **PBDTSe-FBT**, f) **PBDTSe-FFBT** tetramers. ESP for the acceptor units in the middle of the chain for g) **PBDTSe-BT**, h) **PBDTSe-FBT**, i) **PBDTSe-FFBT**.

443 °C, 437 °C and 400 °C, respectively. The synthesized polymers did not display any phase transition up to 300 °C.

3.3. Computational Results

HOMO, HOMO-1, HOMO-2 orbital surfaces given in Fig. 1a-c showed that HOMO orbitals were distributed along the chain similar to previous studies. [30–32] LUMO orbitals were highly localized on the acceptor groups. LUMO, LUMO+1 and LUMO+2 are positioned on different acceptor units due to different chemical environments in the middle part and end groups of the tetramers which is also valid for HOMO, HOMO+1 and HOMO+2 frontier orbitals showing a complementary behavior along the chain. Although their distribution for **PBDTSe-BT, PBDTSe-FBT** and **PBDTSe-FFBT** looks similar, there are small differences in the details. LUMO orbitals were extended to the fluorine atoms in the acceptor unit for **PBDTSe-FBT** and **PBDTSe-FFBT**. In addition, the extension of HOMO orbitals on the acceptor units has a different shape and distribution for different copolymers. The difference in the electron density distribution can be seen more clearly from the ESP surface mapped onto the model structures where electron rich sites were concentrated on the donor and bridge groups, displayed in red color, while electron deficient sites were concentrated on the acceptor and alkyl side chains, displayed in blue color (Fig. 1d-f). Weak extension of electron rich sites on the **PBDTSe-BT** acceptor, especially on its phenyl group of benzothiadiazole, was not observed after fluorine substitution in **PBDTSe-FBT** and **PBDTSe-FFBT**. Both phenyl and thiadiazole rings donate electrons upon the substitution of fluorine atoms which leads to the enhanced acceptor capacity for the fluorine substituted benzothiadiazole unit in the polymer backbone (Fig. 1g-i).

Table 2
Results of DFT calculations for the structural and electronic properties of **PBDTSe-BT**, **PBDTSe-FBT** and **PBDTSe-FFBT** tetramers. (Energies are in eV, dipole moments are debye, polarizabilities are in a.u.).

	HOMO	LUMO	E_g	E_g^{op}	VIP	AIP	VEA	AEA
PBDTSe-BT	−4.98	−2.98	−2.00	1.68	5.44	5.36	−2.50	−2.55
PBDTSe-FBT	−5.01	−3.04	−1.97	1.66	5.46	5.39	−2.56	−2.60
PBDTSe-FFBT	−5.05	−3.07	−1.99	1.68	5.51	5.44	−2.59	−2.63

	λ_{reorg}	π_{del}	$\delta_{Acceptor}$	θ (A-B)	μ	α	$\Delta\alpha$	β
PBDTSe-BT	0.142	5320	0.07 (−0.30)	8.79	0.16	3778	5263	14,978
PBDTSe-FBT	0.139	3734	−0.02 (−0.09)	3.76	7.26	3801	5328	18,361
PBDTSe-FFBT	0.138	540	−0.13 (0.11)	1.70	0.29	3787	5299	23,409

DFT calculations showed that HOMO energies have more negative values by incorporation of the fluorine atoms as observed experimentally that is relevant for the enhanced V_{OC} values (Table 2). LUMO levels also have lower values that result in the close band gap values for polymers where **PBDTSe-FBT** has slightly lower band gap values. Although calculations predicted close E_g^{opt} values with experiments, there is a difference in their order at experimental and theoretical results which is mainly due to the molecular weight difference and lack of intermolecular interactions in the computational results that can affect electronic structure by fluorine substitution. Vertical and adiabatic ionization potentials (VIP and AIP) were increased and electron affinities (VEA and AEA) were decreased due to improved electronegativities by fluorine incorporation. Hole reorganization energies ($\boldsymbol{\lambda_{reorg}}$) that indicate ease of hole mobility along the chain were low for all chains and slightly improved by fluorine incorporation. The most significant change was observed in the delocalization or resonance energy ($\boldsymbol{\pi_{del}}$) where fluorine substitution decreased π-electron energy in the conjugated polymer backbone, particularly from the benzodithiophene acceptor rings. This is supported by the electrostatic potential surfaces in Fig. 1. This hypothesis was tested by the calculation of the total average atomic charges on the acceptor. The average total atomic charge on acceptor units ($\boldsymbol{\delta_{Acceptor}}$) obtain more negative value by fluorine substitution. However, total atomic charges only on the acceptor ring excluding hydrogens and fluorine atoms are increasing and became a positive number as given in parenthesis which indicates improved acceptor potential. Although fluorine atoms attracted electrons from other units and increase overall electron density on the acceptor unit, this electron density is concentrated on the fluorine atoms and total electron density on the acceptor ring is decreased. The average torsional angle between acceptor and bridging units ($\boldsymbol{\theta}$ **(A-B)**) presented that planarity of the chains was improved by fluorine substitution that can lead to the increased quinoid character, better chain packing leading to the enhanced intra-charge transport and inter-chain hopping. [51] It should be noted that the two sides of **PBDTSe-FBT** acceptor were not identical where the fluorine side has a lower dihedral angle compared to the side hydrogen side. This asymmetrical structure of **PBDTSe-FBT** leads to the higher dipole moment (μ,), static polarizability (α) and anisotropy in the polarizability ($\Delta\alpha$) compared to **PBDTSe-BT** and **PBDTSe-FFBT**. First order hyperpolarizability (β) which is a measure for the induced dipole formation in an electric field that was reported as an indication for decreased bond length alternation in conjugated chains with higher β values. [36,52] Increasing β values by fluorine substitution points out enhanced donor, bridge and acceptor unit coupling with lower bond length alternation.

3.4. Electrochemical properties

The cyclic voltammetry (CV) measurements were executed for **PBDTSe-BT, PBDTSe-FBT** and **PBDTSe-FFBT** between the suitable potentials to investigate the redox performances of the resulted polymers at a constant 100 mV/s scan rate at room temperature. The experimental study of CV was conducted via a three-electrode setup in which indium tin oxide (ITO) was used as the working electrode, Ag wire as the reference electrode and Pt as the counter electrode. Acetonitrile (ACN) was the solvent and tetrabutylammoniumhexafluorophosphate ($TBAPF_6$) was the supporting electrolyte during the measurements. Doping/dedoping potentials, onset oxidation potentials (E_{onset}^{ox}) and onset reduction potentials (E_{onset}^{red}) of polymers were explored from the cyclic voltammograms. As depicted in Fig. 2, all polymers showed both p-dopable and n-dopable character. All the electrochemical properties were summarized in Table 3. The E_{onset}^{ox} were measured as 0.5 eV, 0.77 eV and 0.81 eV while E_{onset}^{red} were detected as −1.09 eV, −0.93 eV and −1.16 eV for **PBDTSe-BT, PBDTSe-FBT** and **PBDTSe-FFBT** respectively. The electron-withdrawing nature of the fluorine atom may be the result of the variation in the oxidation potential of the polymers. These electron-withdrawing effect results in lower electron density on benzothiadiazole moiety in the polymer backbone of **PBDTSe-BT** and **PBDTSe-FFBT**. Therefore, doping/dedoping processes occur at higher oxidation potentials. Moreover, high occupied molecular orbital (HOMO) and low occupied molecular orbital (LUMO) energy levels were deduced from the onset oxidation potentials and onset reduction potentials of the corresponding polymers according to the following equations;

$$HOMO = -(4.75 + E_{onset}^{ox})$$

$$LUMO = -(4.75 + E_{onset}^{red})$$

Standard Hydrogen Electrode (SHE) vs. vacuum level was adopted as 4.75 eV. The electronic band gaps (E_g^{el}) of **PBDTSe-BT, PBDTSe-FBT** and **PBDTSe-FFBT** were calculated from the energy level difference between HOMO and LUMO. The following equation was used for the calculation of the electronic band gaps of polymers;

$$E_g^{el} = \text{HOMO} - \text{LUMO}$$

HOMO energy levels for **PBDTSe-BT, PBDTSe-FBT** and **PBDTSe-FFBT** were found as −5.28 eV, −5.52 eV and −5.56 eV whereas LUMO energy levels were calculated as −3.65 eV, −3.82 eV and −3.59 eV, respectively. Therefore, the electronic band gaps of **PBDTSe-BT, PBDTSe-FBT** and **PBDTSe-FFBT** were deduced to be 1.63 eV, 1.70 eV and 1.97 eV. The HOMO energy level of the synthesized polymers decreases dramatically upon fluorine substitution with approximately 0.3 eV energy difference between the difluorinated (**PBDTSe-FFBT**) and the non-fluorinated (**PBDTSe-BT**) polymers. The deeper HOMO energy level of the polymer was associated with the strong electron-withdrawing characteristic of benzothiadiazole acceptor and weak electron-donating nature of alkylselenophene side chain which has π-conjugation to BDT moiety. Moreover, the electronic band gap of non-fluorinated

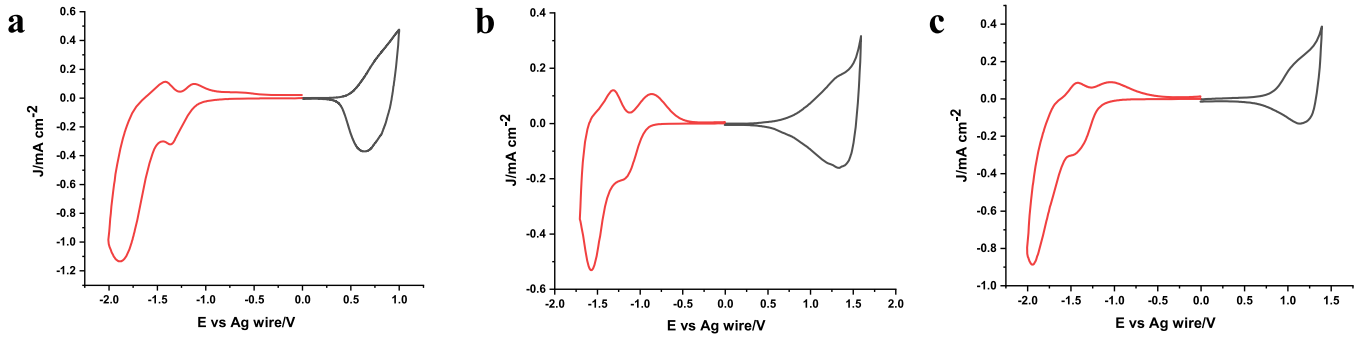

Fig. 2. Single scan cyclic voltammograms of polymers a) **PBDTSe-BT**, b) **PBDTSe-FBT**, and c) **PBDTSe-FFBT** in 0.1 M $TBAPF_6$/ACN electrolyte solution at 100 mV s^{-1} scan rate.

Table 3
Summary of electrochemical and optical properties of polymers.

	$E_{p\text{-doping}}$/V	$E_{p\text{-dedoping}}$/V	$E_{n\text{-doping}}$/V	$E_{n\text{-dedoping}}$/V	E^{ox}_{onset}/V	E^{red}_{onset}/V
PBDTSe-BT	0.75	0.64	−1.36/−1.88	−1.12/−1.42	0.53	−1.10
PBDTSe-FBT	1.35	1.33	−1.18/−1.57	−0.87/−1.32	0.77	−0.93
PBDTSe-FFBT	1.20	1.16	−1.47/−1.95	−1.05/−1.42	0.81	−1.16

	HOMO/eV	LUMO/eV	E_g^{ec}/eV	λ_{max}/nm	λ_{onset}/nm	E_g^{op}/eV
PBDTSe-BT	−5.28	−3.65	1.63	620	763	1.62
PBDTSe-FBT	−5.52	−3.82	1.70	600	754	1.65
PBDTSe-FFBT	−5.56	−3.59	1.97	590	745	1.67

polymer **PBDTSe-BT** exhibited lower band gap energy than fluorinated **PBDTSe-FBT** and **PBDTSe-FFBT** which may arise from the strong electronegativity of fluorine atom and enhanced inter-/intramolecular interaction among polymer backbones. [53–55]

While different HOMO levels are obtained from theoretical and experimental methods for **PBDTSe-BT, PBDTSe-FBT** and **PBDTSe-FFBT** conjugated polymers, these values reveal the same trend; i.e., with the introduction of F atoms onto the benzothiadiazole moiety the HOMO level of polymers can be diminished, and also the number of fluorination on these polymers has a synergetic impact on reducing the HOMO level. [56]

3.5. Spectroelectrochemical properties

In order to investigate the spectroelectrochemical properties of the polymers, a three-electrode system was used. **PBDTSe-BT, PBDTSe-FBT** and **PBDTSe-FFBT** were dissolved in chloroform and deposited onto ITO coated glass substrate via spray coating at room temperature. All polymers have good solubility in chloroform and homogenous solutions were obtained for the spectroelectrochemical analysis. The analysis of three polymers was performed with UV–Vis-NIR spectrophotometer via step by step increment of the applied potential in 0.1 M $TBAPF_6$/ACN solution. Constant potentials were carried out to remove the charges or ions trapped into polymers and record the neutral states correctly before applying the oxidation potentials. Absorption spectra were obtained by stepwise oxidation and while the neutral state absorptions (λ_{max}) were steadily declining, polarons (radical cations) and bipolarons (bications) absorption bands were observed in the NIR region as expected. The absorption behaviors of polymers in the UV–Vis region give essential information, especially for organic solar cell applications. For this purpose, optical band gaps (E_g^{op}) and maximum absorption wavelengths (λ_{max}) of the polymers were obtained from Fig. 3 and all data were summarized in Table 3. The λ_{max} values were found as 620 nm, 600 nm and 590 nm for **PBDTSe-BT, PBDTSe-FBT** and **PBDTSe-FFBT**, accordingly. The optical bandgaps (E_g^{op}) were calculated from the onset point of the lowest energy π–π^* transitions (λ_{onset}) in the UV–Vis-NIR absorption spectrum of the polymer thin films by using the following equation;

$$E_g^{op} = \frac{1241}{\lambda_{onset}}$$

The band gaps (E_g^{op}) were calculated as 1.62 eV, 1.65 eV and 1.67 eV for **PBDTSe-BT, PBDTSe-FBT** and **PBDTSe-FFBT** correspondingly. The backbone fluorination slightly increased the optical band gaps and the changes in the absorption spectra clearly reveal the effect of substitution of fluorine atom. Similar results have also been published for fluorine atom substituted conjugated polymer by other groups. [54,55,57,58]

All the polymers displayed an absorption shoulder peak in thin-film state and the existence of strong intermolecular interactions caused by better π–π stacking between the neighbor polymer chains might be the reason for this phenomenon. On the other hand, when fluorine atoms are substituted to the polymer backbone, **PBDTSe-FFBT** showed pronounced absorption shoulder around 650 nm demonstrating strong polymer aggregation at room temperature. Therefore, the strong aggregation in **PBDTSe-FFBT** may be caused by intermolecular interactions of F…F, C-F…H, and C-F…π_F. [59,60] Due to the introduction of fluorine atoms leading to more pronounced aggregation, **PBDTSe-FFBT** demonstrates a lower wavelength in the absorption spectrum compared to **PBDTSe-FBT** and **PBDTSe-BT** which may result in a slightly larger band gap of 1.67 eV.

3.6. Photovoltaic Performance

BHJ photovoltaic devices of these three polymers were fabricated to explore and analyze the influence of the substituting fluorine atom on the resultant photovoltaic performance. Organic solar devices with standard configuration, ITO/PEDOT:PSS/Polymer:$PC_{71}BM$/LiF/Al, were employed using **PBDTSe-BT, PBDTSe-FBT** and **PBDTSe-FFBT** as donors and $PC_{71}BM$ as an acceptor counterpart into the active layer of the devices. While determining the processing solvent of the active layer, different weight ratios of the polymer to $PC_{71}BM$ and the concentration of the active layer were investigated. Moreover, a small amount of 1,8-diiodooctane (DIO) was used to optimize the photovoltaic

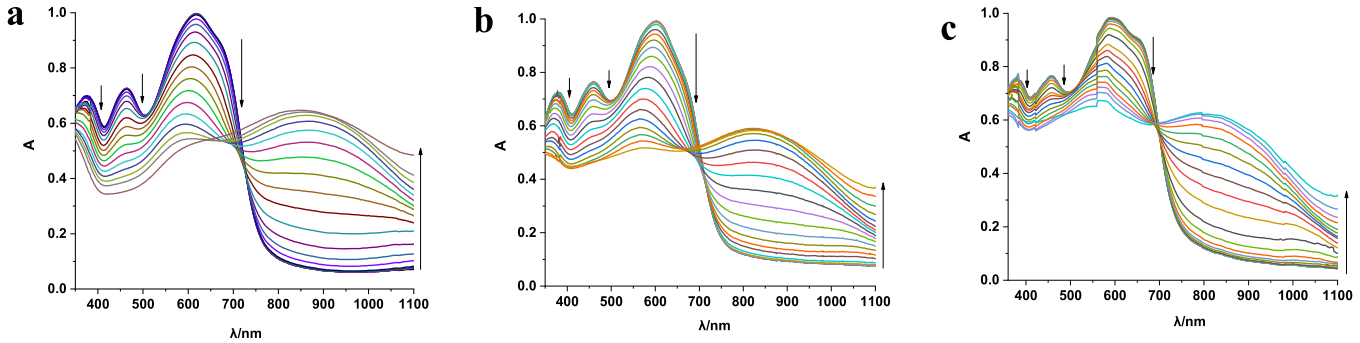

Fig. 3. Normalized UV–Vis-NIR absorption spectra of thin film of a) **PBDTSe-BT**, b) **PBDTSe-FBT**, and c) **PBDTSe-FFBT** upon oxidative doping potentials in 0.1 M $TBAPF_6$/ACN electrolyte solution.

Table 4
Summary of photovoltaic studies of **PBDTSe-BT**, **PBDTSe-FBT** and **PBDTSe-FFBT**.

	Polymer:$PC_{71}BM$/w:w	J_{sc}/mA cm^{-2}	V_{oc}/V	FF%	PCE%	Treatment
PBDTSe-BT	1:4 (4%)[a]	5.43	0.67	39.4	1.43	–
	1:4 (4%)[b]	4.84	0.67	43.9	1.42	–
	1:4 (4%)[c]	6.10	0.67	41.9	1.71	–
	1:4 (4%)[c]	5.67	0.66	45.6	1.70	1% DIO
	1:4 (4%)[c]	**6.58**	**0.66**	**55.3**	**2.39**	**2% DIO**
	1:4 (4%)[c]	6.22	0.67	54.0	2.26	3% DIO
	1:4 (4%)[c]	6.48	0.67	52.8	2.29	2% DIO, MeOH
PBDTSe-FBT	1:2 (3%)[a]	3.34	0.65	39.1	0.85	–
	1:2 (3%)[b]	6.17	0.66	36.1	1.47	–
	1:2 (3%)[c]	6.00	0.65	39.2	1.53	–
	1:2 (3%)[c]	7.09	0.68	34.0	1.64	2% DIO
	1:2 (3%)[c]	**7.23**	**0.67**	**34.6**	**1.68**	**3% DIO**
	1:2 (3%)[c]	6.16	0.65	31.1	1.25	4% DIO
PBDTSe-FFBT	1:1 (2%)[a]	4.99	0.70	38.8	1.36	–
	1:1 (2%)[b]	5.75	0.70	49.2	1.99	–
	1:1 (2%)[c]	6.40	0.70	50.4	2.26	–
	1:1 (2%)[c]	6.15	0.72	50.5	2.23	2% DIO
	1:1 (2%)[c]	**7.24**	**0.72**	**50.6**	**2.63**	**3% DIO**
	1:1 (2%)[c]	6.76	0.71	47.4	2.28	4% DIO

[a] Spin coating rate of 500 rpm.
[b] Spin coating rate of 750 rpm.
[c] Spin coating rate of 1000 rpm.

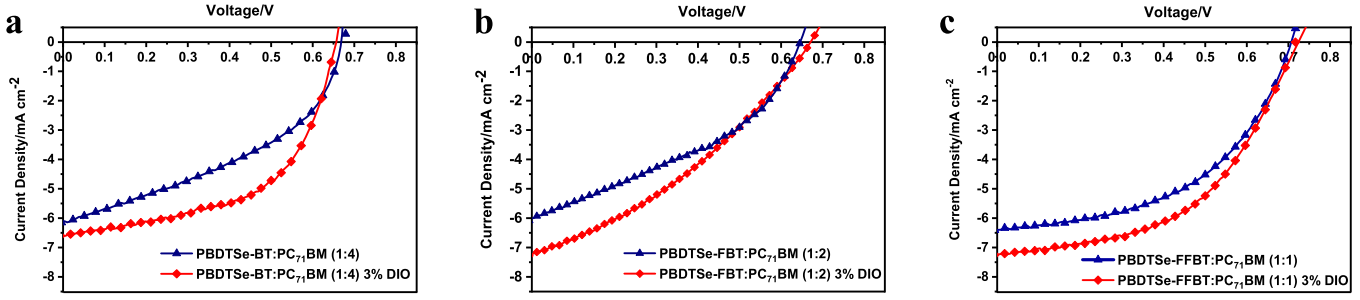

Fig. 4. Current density-voltage curves of OSCs based on a) **PBDTSe-BT**:PC $_{71}$BM, b) **PBDTSe-FBT**:PC $_{71}$BM, and c) **PBDTSe-FFBT**:PC $_{71}$BM without additive and with additive in the active layer.

performance of the devices. The thicknesses of the active layers were optimized by altering the spin coating rate which was found as 1000 rpm for all polymers. The blends based on **PBDTSe-BT** were dissolved in 1,2-dichlorobenzene (*o*-DCB) and **PBDTSe-FBT** and **PBDTSe-FFBT** based blends were dissolved in chlorobenzene (CB). The photovoltaic parameters, including open-circuit voltage (V_{OC}), short circuit current density (J_{SC}), fill factor (FF) and power conversion efficiency (PCE) of the devices using polymers **PBDTSe-BT, PBDTSe-FBT** and **PBDTSe-FFBT** are summarized in Table 4. Fig. 4 shows the resultant current density-voltage (J-V) plots of the most efficient devices, which were investigated under AM 1.5 G simulated solar illumination at an irradiation intensity of 100 mW cm^{-2}.

Among all three polymers, difluorinated **PBDTSe-FFBT**:$PC_{71}BM$ revealed the highest photovoltaic performance achieving 2.63%, with J_{SC} of 7.24 mA cm^{-2}, V_{OC} of 0.72 V and FF of 50.6%. Whereas **PBDTSe-BT**:$PC_{71}BM$ exhibited the best PCE as 2.39%, and the device reached the highest efficiency up to 1.68% for **PBDTSe-FBT**:$PC_{71}BM$. Polymer $PC_{71}BM$ weight ratio of the blend in the active layer is essential to optimize the photovoltaic parameters. Since the function of the acceptor material in the active layer is associated with the charge transport, electron and hole mobilities were balanced by changing the weight ratio of the electron accepting material PCBM in the blend. As a result of this enhancement, efficient charge separation occurs and more separated charge carriers can be transported and collected at the

proper electrodes, which arises higher PCE. However, this increase of the acceptor material causes a decrease in the content of the donor material, which plays a vital role in the absorption of sunlight in the active layer. Therefore, the optimization of the weight ratios of the donor and acceptor materials is an essential process to obtain efficient PCE. Consequently, the best device performances were found with a blend ratio of 1:4 (w/w), 1:2 (w/w) and 1:1 (w/w) for **PBDTSe-BT, PBDTSe-FBT** and **PBDTSe-FFBT**, respectively.

Further improvement in the PCE was observed by the addition of a trace amount of DIO to the active layer of the OSC. With the addition of 1% DIO to the active layer, device efficiency of **PBDTSe-BT**:$PC_{71}BM$ (1:4, 4%) remained unchanged while an improvement from 41.9% to 45.6% in the FF% obtained. An increase in the Jsc from 5.67 to 6.58 mA cm^{-2} and FF from 45.6% to 55.3% was observed by the addition of 2% DIO resulting 2.39% of PCE. Further DIO and methanol treatment for **PBDTSe-BT** resulted in lower photovoltaic parameters. The studies for the optimum amount of the DIO were carried out for **PBDTSe-FBT** and **PBDTSe-FFBT**. The results showed that the best device efficiency was found 1.68% for **PBDTSe-FBT** and 2.63% for **PBDTSe-FFBT** with the addition of 3% DIO. It is believed that the donor can form pure and ordered self-assembly phases in the film due to the high boing point property of DIO, which promotes and stimulates the generation of crystal structures. [61]

The substitution of the fluorine atom along the conjugation backbone provides effective tuning of the molecular energy levels as well as enhanced intramolecular interactions. [62] DFT calculations and experimental results indicated that **PBDTSe-FFBT** including two F atoms into its polymer backbone has a deeper HOMO level in regards to **PBDTSe-BT** and **PBDTSe-FBT**. Therefore, an increase in V_{OC} of the best solar cell device was observed that might lead to higher PCE of the solar cell. Moreover, according to the DFT calculations, hole mobility along the polymers chain slightly improved by F incorporation due to increased hole reorganization energies ($\boldsymbol{\lambda_{reorg}}$) listed in Table 2. Higher charge carrier mobility may also be one of the reasons for the high photovoltaic performance of **PBDTSe-FFBT** based solar cell.

Overall, the efficiencies of the synthesized polymers were moderate in this work, however, several factors such as HOMO-LUMO energy levels, device structure, the molecular weight of the polymers, band gap etc. affect the device efficiency. [63–65] Although the benzothiadiazole-based conjugated polymers exhibit great properties for photovoltaics, the molecular weight of the polymer was recognized to be significant. [66,67] High molecular weight of the polymers usually form favorable film morphologies when mixed with PCBM leading to efficient charge separation.

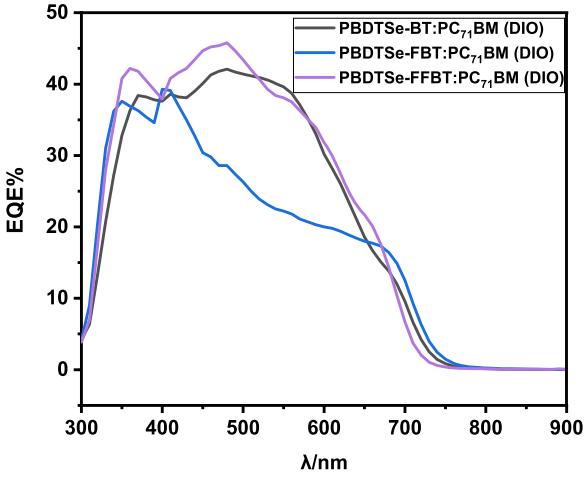

Fig. 5. EQE curves for the best performance solar cells.

[68] Due to the insufficient growth of the polymer chains during the Stille cross-coupling polymerization, the low molecular weight of polymers was synthesized. Therefore, the lower PCEs were revealed for **PBDTSe-BT, PBDTSe-FBT** and **PBDTSe-FFBT.**

External quantum efficiency (EQE) curves of the devices based on **PBDTSe-BT, PBDTSe-FBT** and **PBDTSe-FFBT** without DIO addition and with DIO addition via using the optimum conditions were shown in Fig. 5. The EQEs for the best device performances were observed over the wavelength range of 300–750 nm which are in agreement with the absorption spectra of the polymers. The highest EQE% values were found as 42.1%, 39.3% and 45.8% for **PBDTSe-BT, PBDTSe-FBT** and **PBDTSe-FFBT** with the addition of DIO, respectively.

3.7. Morphology studies

In order to gain information about the morphology and topography of the photo-active layer of OSC devices, transmission electron microscopy (TEM) and atomic force microscopy (AFM) were utilized. TEM images of **PBDTSe-BT, PBDTSe-FBT** and **PBDTSe-FFBT** polymers as the active layers of best OSC with DIO addition were shown in Fig. 6, respectively. As seen from Fig. 6, **PBDTSe-BT, PBDTSe-FBT** and **PBDTSe-FFBT** based solar cells display homogenous and nanoscale phase separation with DIO treatment. [69] As mentioned before in computational results, the torsional angles $\boldsymbol{\theta}$ **(A-B)** decreased with fluorine substitution, which indicates better planarity resulting in improved chain packing and interchain hop-

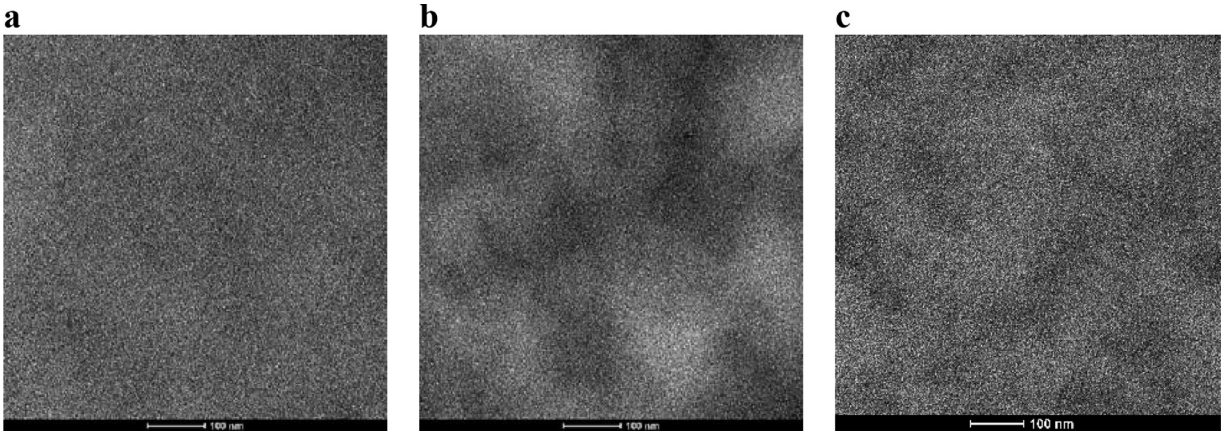

Fig. 6. TEM images of a) **PBDTSe-BT**, b) **PBDTSe-FBT** and c) **PBDTSe-FFBT** based active layers processed with *o*-dcb and DIO.

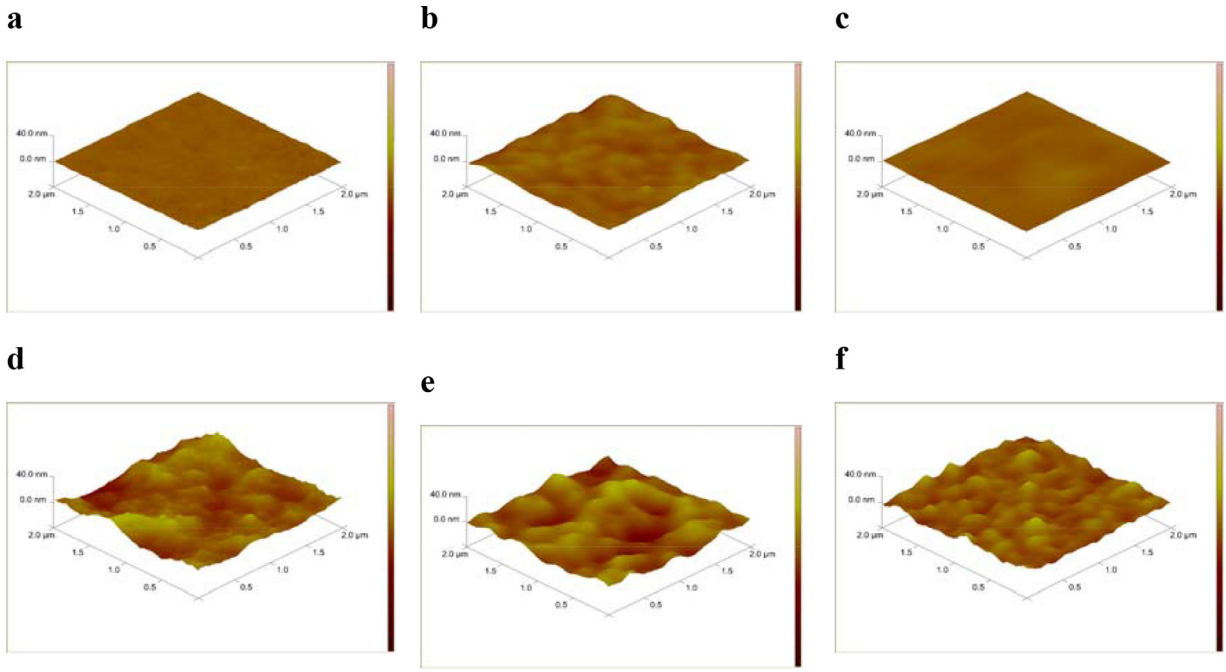

Fig. 7. 3D AFM images of a) **PBDTSe-BT**, b) **PBDTSe-FBT** and c) **PBDTSe-FFBT** without the additive DIO; d) **PBDTSe-BT**, e) **PBDTSe-FBT** and f) **PBDTSe-FFBT** with the additive DIO.

ping. Therefore, F substitution promotes the exciton separation and charge transportation causing an increase in J_{SC} and FF. [70,71]

The 3D AFM height images of the most efficient devices without DIO and with DIO are shown in Fig. 7. The root mean square roughness of the blend of **PBDTSe-BT, PBDTSe-FBT** and **PBDTSe-FFBT** with PCBM were calculated as 0.66 nm, 1.81 nm and 0.97 nm as cast polymer blends; 4.61 nm, 5.43 nm and 3.21 nm for DIO treatment, respectively. The active layer thickness values were found as 107.6 nm, 150.7 nm and 120.2 nm without DIO addition; 123.5 nm, 117.0 nm and 64.7 nm with DIO addition, correspondingly. As can be seen from Fig. 7a and Fig. 7c, the blend of the **PBDTSe-BT** and **PBDTSe-FFBT** had the lowest roughnesses. As DIO was added to the active layer, the roughness values increased significantly. With the addition of DIO, which enhances the solubility of PCBM, PCBM aggregates tend to form near the surface resulting in an increase in surface roughness. [72]

4. Conclusion

In conclusion, to investigate the effect of the number of fluorine atoms substituted to the benzothiadiazole, 2-ethylhexyl selenophene substituted benzodithiophene monomer (BDTSe) and benzothiadiazole monomer with the fluorine substitution were used as the electron rich and the electron deficient units during Stille coupling polymerization, respectively. As a result, a series of new conjugated polymers **PBDTSe-BT, PBDTSe-FBT** and **PBDTSe-FFBT** were developed and specifically examined for their photovoltaic properties. The resulting polymers showed good thermal stability with T_d higher than 400 °C. All polymers showed narrow E_g^{op} of 1.62 eV, 1.65 eV and 1.67 eV with deep-lying HOMO energy levels of −5.28 eV, −5.52 eV and −5.56 eV, respectively. With the incorporation of fluorine atom, HOMO energy level of the **PBDTSe-FBT** and **PBDTSe-FFBT** were decreased compared to the polymer **PBDTSe-BT**. DFT studies were conducted for these polymers to get more information about the electronic and optical parameters. According to the computational studies, fluorine atom substituted benzothiadiazole moiety improved the electron accepting ability of the acceptor unit in the polymer backbone. Hole reorganization energies, the delocalization energies and average torsional angles were also affected by fluorine substitution which result in promoted PCEs. The optimization of the photovoltaic properties of the polymers was conducted with different weight ratios of polymer:$PC_{71}BM$, the concentration of the active layer, additive volume ratio and thickness. For the optimized active layer of **PBDTSe-FFBT**, J_{SC} of 7.24 mA cm^{-2}, V_{OC} of 0.72 V and FF of 50.6% was found, resulting in a PCE of 2.63%. The fluorine substitution on the benzothiadiazole unit was shown to influence the thin-film morphology of the organic solar cell with $PC_{71}BM$, and therefore an optimized phase separation was achieved with the assistance of a small molecule processing additive, DIO. It should be noted that **PBDTSe-FBT** had one fluorine atom substituted to the polymer backbone resulting asymmetrical structure that may influence the photovoltaic performance of the solar cell. It is concluded that conjugated polymers with fluorine substituent on the acceptor moiety have an impact on the solar cell performances.

Credit author statement

STA: material syntheses and characterizations, **EB**: performed all device fabrications and characterizations, **STA, DK, EB, GHO** and **YAU**: conceived and planned the experiments, **EY**: developed the theory and performed computations, **STA, LT** and **AC**: took the lead in writing the manuscript, **AC**: provided critical feedback and helped shape the research, analysis, and manuscript

Declaration of Competing Interest

The authors declare that they have no known competing financial interests or personal relationships that could have appeared to influence the work reported in this paper.

Acknowledgments

This study was supported by the Scientific and Technological Research Council of Turkey (TÜBİTAK) (Project No: 115M036). We express our sincere thanks for their financial support.

Erol Yıldırım gratefully acknowledges support from 2232 International Fellowship for Outstanding Researchers Program of TÜBİTAK (Project No: 118C251)

References

[1] Y. Liang, Z. Xu, J. Xia, S.T. Tsai, Y. Wu, G. Li, C. Ray, L. Yu, For the bright future-bulk heterojunction polymer solar cells with power conversion efficiency of 7.4%, Adv. Mater. 22 (2010) E135–E138, doi:10.1002/adma.200903528.

[2] H. Yao, L. Ye, H. Zhang, S. Li, S. Zhang, J. Hou, Molecular design of benzodithiophene-based organic photovoltaic materials, Chem. Rev. 116 (2016) 7397–7457, doi:10.1021/acs.chemrev.6b00176.

[3] M. Liu, Y. Gao, Y. Zhang, Z. Liu, L. Zhao, Quinoxaline-based conjugated polymers for polymer solar cells, Polym. Chem. 8 (2017) 4613–4636, doi:10.1039/c7py00850c.

[4] X. Ma, J. Wang, J. Gao, Z. Hu, C. Xu, X. Zhang, F. Zhang, Achieving 17.4% Efficiency of ternary organic photovoltaics with two well-compatible non-fullerene acceptors for minimizing energy loss, Adv. Energy Mater. 10 (2020) 1–9, doi:10.1002/aenm.202001404.

[5] Q. Liu, Y. Jiang, K. Jin, J. Qin, J. Xu, W. Li, J. Xiong, J. Liu, Z. Xiao, K. Sun, S. Yang, X. Zhang, L. Ding, 18% Efficiency organic solar cells, Sci. Bull. 65 (2020) 272–275, doi:10.1016/j.scib.2020.01.001.

[6] S. Chen, T. Yan, B. Fanady, W. Song, J. Ge, Q. Wei, R. Peng, G. Chen, Y. Zou, Z. Ge, High efficiency ternary organic solar cells enabled by compatible dual-donor strategy with planar conjugated structures, Sci. China Chem. 63 (2020) 917–923, doi:10.1007/s11426-020-9736-6.

[7] H. Hwang, C. Park, D.H. Sin, E. Song, K. Cho, High absorption coefficient π-conjugation-extended donor-acceptor copolymers for ternary-blend solar cells, Org. Electron. 83 (2020) 105738, doi:10.1016/j.orgel.2020.105738.

[8] A. Karki, J. Vollbrecht, A.L. Dixon, N. Schopp, M. Schrock, G.N.M. Reddy, T.Q. Nguyen, Understanding the high performance of over 15% efficiency in single-junction bulk heterojunction organic solar cells, Adv. Mater. 31 (2019) 1903868, doi:10.1002/adma.201903868.

[9] B. Walker, J. Liu, C. Kim, G.C. Welch, J.K. Park, J. Lin, P. Zalar, C.M. Proctor, J.H. Seo, G.C. Bazan, T.Q. Nguyen, Optimization of energy levels by molecular design: Evaluation of bis-diketopyrrolopyrrole molecular donor materials for bulk heterojunction solar cells, Energy Environ. Sci. 6 (2013) 952–962, doi:10.1039/c3ee24351f.

[10] X. Yang, J. Loos, Toward high-performance polymer solar cells: the importance of morphology control, Macromol 40 (2007) 1353–1362, doi:10.1021/ma0618732.

[11] B. Fan, D. Zhang, M. Li, W. Zhong, Z. Zeng, L. Ying, F. Huang, Y. Cao, Achieving over 16% efficiency for single-junction organic solar cells, Sci. China Chem. 62 (2019) 746–752, doi:10.1007/s11426-019-9457-5.

[12] Y. Cui, H. Yao, J. Zhang, T. Zhang, Y. Wang, L. Hong, K. Xian, B. Xu, S. Zhang, J. Peng, Z. Wei, F. Gao, J. Hou, Over 16% efficiency organic photovoltaic cells enabled by a chlorinated acceptor with increased open-circuit voltages, Nat. Commun. 10 (2019) 2515, doi:10.1038/s41467-019-10351-5.

[13] L. Meng, Y. Zhang, X. Wan, C. Li, X. Zhang, Y. Wang, X. Ke, Z. Xiao, L. Ding, R. Xia, H.L. Yip, Y. Cao, Y. Chen, Organic and solution-processed tandem solar cells with 17.3% efficiency, Sci. 361 (2018) 1094–1098 (80-.), doi:10.1126/science.aat2612.

[14] K. Borse, R. Sharma, D. Gupta, A. Yella, High-efficiency organic solar cells with solution processable non-fullerene acceptor as an interlayer, IEEE J. Photovoltaics. 9 (2019) 1266–1272, doi:10.1109/JPHOTOV.2019.2924400.

[15] D. Zimmermann, C. Sprau, J. Schröder, V.G. Gregoriou, A. Avgeropoulos, C.L. Chochos, A. Colsmann, S. Janietz, H. Krüger, Synthesis of D-π-A-π type benzodithiophene-quinoxaline copolymers by direct arylation and their application in organic solar cells, J. Polym. Sci. Part A Polym. Chem. 56 (2018) 1457–1467, doi:10.1002/pola.29027.

[16] K. He, P. Kumar, Y. Yuan, Z. Zhang, X. Li, H. Liu, J. Wang, Y. Li, A wide bandgap polymer donor composed of benzodithiophene and oxime-substituted thiophene for high-performance organic solar cells, ACS Appl. Mater. Interfaces. 13 (2021) 26441–26450, doi:10.1021/acsami.1c02442.

[17] R.S. Ashraf, I. Meager, M. Nikolka, M. Kirkus, M. Planells, B.C. Schroeder, S. Holliday, M. Hurhangee, C.B. Nielsen, H. Sirringhaus, I. McCulloch, Chalcogenophene comonomer comparison in small band gap diketopyrrolopyrrole-based conjugated polymers for high-performing field-effect transistors and organic solar cells, J. Am. Chem. Soc. 137 (2015) 1314–1321, doi:10.1021/ja511984q.

[18] H.Y. Chen, S.C. Yeh, C.T. Chen, C.T. Chen, Comparison of thiophene- and selenophene-bridged donor-acceptor low band-gap copolymers used in bulk-heterojunction organic photovoltaics, J. Mater. Chem. 22 (2012) 21549–21559, doi:10.1039/c2jm33735e.

[19] D.J. Crouch, P.J. Skabara, J.E. Lohr, J.J.W. McDouall, M. Heeney, I. McCulloch, D. Sparrowe, M. Shkunov, S.J. Coles, P.N. Horton, M.B. Hursthouse, Thiophene and selenophene copolymers incorporating fluorinated phenylene units in the main chain: synthesis, characterization, and application in organic field-effect transistors, Chem. Mater. 17 (2005) 6567–6578, doi:10.1021/cm051563i.

[20] W.H. Chang, L. Meng, L. Dou, J. You, C.C. Chen, Y. Yang, E.P. Young, G. Li, A selenophene containing benzodithiophene- alt -thienothiophene polymer for additive-free high performance solar cell, Macromol. 48 (2015) 562–568, doi:10.1021/ma502132t.

[21] N. Chakravarthi, K. Kranthiraja, M. Song, K. Gunasekar, P. Jeong, S.J. Moon, W. Suk Shin, I.N. Kang, J.W. Lee, S.H. Jin, New alkylselenyl substituted benzodithiophene-based solution-processable 2D π-conjugated polymers for bulk heterojunction polymer solar cell applications, Sol. Energy Mater. Sol. Cells. 122 (2014) 136–145, doi:10.1016/j.solmat.2013.11.019.

[22] J.M. Jiang, P. Raghunath, H.K. Lin, Y.C. Lin, M.C. Lin, K.H. Wei, Location and number of selenium atoms in two-dimensional conjugated polymers affect their band-gap energies and photovoltaic performance, Macromol 47 (2014) 7070–7080, doi:10.1021/ma501720k.

[23] Y.S. Byun, J.H. Kim, J.B. Park, I.N. Kang, S.H. Jin, D.H. Hwang, Full donor-type conjugated polymers consisting of alkoxy- or alkylselenophene-substituted benzodithiophene and thiophene units for organic photovoltaic devices, Synth. Met. 168 (2013) 23–30, doi:10.1016/j.synthmet.2013.02.013.

[24] Q. Fan, U.A. Méndez-Romero, X. Guo, E. Wang, M. Zhang, Y. Li, Fluorinated photovoltaic materials for high-performance organic solar cells, Chem. - An Asian J. 14 (2019) 3085–3095, doi:10.1002/asia.201900795.

[25] N. Leclerc, P. Chávez, O.A. Ibraikulov, T. Heiser, P. Lévêque, Impact of backbone fluorination on π-conjugated polymers in organic photovoltaic devices: a review, Polymers (Basel) 8 (2016) 11, doi:10.3390/polym8010011.

[26] H.C. Chen, Y.H. Chen, C.C. Liu, Y.C. Chien, S.W. Chou, P.T. Chou, Prominent short-circuit currents of fluorinated quinoxaline-based copolymer solar cells with a power conversion efficiency of 8.0%, Chem. Mater. 24 (2012) 4766–4772, doi:10.1021/cm302861s.

[27] A.C. Stuart, J.R. Tumbleston, H. Zhou, W. Li, S. Liu, H. Ade, W. You, Fluorine substituents reduce charge recombination and drive structure and morphology development in polymer solar cells, J. Am. Chem. Soc. 135 (2013) 1806–1815, doi:10.1021/ja309289u.

[28] N. Wang, Z. Chen, W. Wei, Z. Jiang, Fluorinated benzothiadiazole-based conjugated polymers for high-performance polymer solar cells without any processing additives or post-treatments, J. Am. Chem. Soc. 135 (2013) 17060–17068, doi:10.1021/ja409881g.

[29] H. Hwang, H. Ko, S. Park, S.R. Suranagi, D.H. Sin, K. Cho, Fluorine-functionalization of an isoindoline-1,3-dione-based conjugated polymer for organic solar cells, Org. Electron. 59 (2018) 247–252, doi:10.1016/j.orgel.2018.05.009.

[30] K. Kawashima, T. Fukuhara, Y. Suda, Y. Suzuki, T. Koganezawa, H. Yoshida, H. Ohkita, I. Osaka, K. Takimiya, Implication of fluorine atom on electronic properties, ordering structures, and photovoltaic performance in naphthobisthiadiazole-based semiconducting polymers, J. Am. Chem. Soc. 138 (2016) 10265–10275, doi:10.1021/jacs.6b05418.

[31] J. Shin, M. Kim, B. Kang, J. Lee, H.G. Kim, K. Cho, Impact of side-chain fluorination on photovoltaic properties: fine tuning of the microstructure and energy levels of 2D-conjugated copolymers, J. Mater. Chem. A. 5 (2017) 16702–16711, doi:10.1039/c7ta04098a.

[32] M.C. Scharber, D. Mühlbacher, M. Koppe, P. Denk, C. Waldauf, A.J. Heeger, C.J. Brabec, Design rules for donors in bulk-heterojunction solar cells - towards 10% energy-conversion efficiency, Adv. Mater. 18 (2006) 789–794, doi:10.1002/adma.200501717.

[33] D. Dang, M. Xiao, P. Zhou, J. Shi, Q. Tao, H. Tan, Y. Wang, X. Bao, Y. Liu, E. Wang, R. Yang, W. Zhu, Manipulating backbone structure with various conjugated spacers to enhance photovoltaic performance of D-A-type two-dimensional copolymers, Org. Electron. 15 (2014) 2876–2884, doi:10.1016/j.orgel.2014.08.022.

[34] A.D. Becke, Density-functional thermochemistry. III. the role of exact exchange, J. Chem. Phys. 98 (1993) 5648–5652, doi:10.1063/1.464913.

[35] P.J. Stephen, F.J. Devlin, C.F. Chabalowski, M.J. Frisch, Ab initio calculation of vibrational absorption and circular dichroism spectra using density functional force fields, J. Phys. Chem. 98 (1994) 11623–11627, doi:10.1021/j100096a001.

[36] S.R. Marder, J.W. Perry, Molecular materials for second-order nonlinear optical applications, Adv. Mater. 5 (1993) 804–815, doi:10.1002/adma.19930051104.

[37] M.J. Frisch, G.W. Trucks, H.B. Schlegel, G.E. Scuseria, M.A. Robb, J.R. Cheeseman, G. Scalmani, V. Barone, G.A. Petersson, H. Nakatsuji, X. Li, M. Caricato, A. Marenich, J. Bloino, B.G. Janesko, R. Gomperts, B. Mennucci, H.P. Hratchian, J.V. Ortiz, A.F. Izmaylov, J.L. Sonnenberg, D. Williams-Young, F. Ding, F. Lipparini, F. Egidi, J. Goings, B. Peng, A. Petrone, T. Henderson, D. Ranasinghe, V.G. Zakrzewski, J. Gao, N. Rega, G. Zheng, W. Liang, M. Hada, M. Ehara, K. Toyota, R. Fukuda, J. Hasegawa, M. Ishida, T. Nakajima, Y. Honda, O. Kitao, H. Nakai, T. Vreven, K. Throssell, J.A. Montgomery Jr., J.E. Peralta, F. Ogliaro, M. Bearpark, J.J. Heyd, E. Brothers, K.N. Kudin, V.N. Staroverov, T. Keith, R. Kobayashi, J. Normand, K. Raghavachari, A. Rendell, J.C. Burant, S.S. Iyengar, J. Tomasi, M. Cossi, J.M. Millam, M. Klene, C. Adamo, R. Cammi, J.W. Ochterski, R.L. Martin, K. Morokuma, O. Farkas, J.B. Foresman, D.J. Fox, Gaussian 09, Revision A.02, Gaussian, Inc., Wallingford CT, 2016.

[38] H.T. Turan, O. Kucur, B. Kahraman, S. Salman, V. Aviyente, Design of donor-acceptor copolymers for organic photovoltaic materials: a computational study, Phys. Chem. Chem. Phys. 20 (2018) 3581–3591, doi:10.1039/c7cp08176f.

[39] E. Aydan Alkan, S. Goker, H. Sarigul, E. Yıldırım, Y.A. Udum, L. Toppare, The impact of [1,2,5]chalcogenazolo[3,4-f]-benzo[1,2,3] triazole structure on the optoelectronic properties of conjugated polymers, J. Polym. Sci. 58 (2020) 956–968, doi:10.1002/pol.20190275.

[40] S.C. Cevher, G. Hizalan, E. Alemdar Yilmaz, D. Cevher, Y. Udum Arslan, L. Toppare, E. Yıldırım, A. Cirpan, A comprehensive study: theoretical and experimental investigation of heteroatom and substituent effects on frontier orbitals and polymer solar cell performances, J. Polym. Sci. 58 (2020) 2792–2806, doi:10.1002/pol.20200513.

[41] M. Yasa, A. Deniz, M. Forough, E. Yildirim, O.P. Cetinkol, Y.A. Udum, L. Toppare, Construction of amperometric biosensor modified with conducting poly-

mer /carbon dots for the analysis of catechol, J. Polym. Sci. 58 (2020) 3336–3348, doi:10.1002/pol.20200647.
[42] J.L. Brédas, D. Beljonne, V. Coropceanu, J. Cornil, Charge-transfer and energy-transfer processes in π-conjugated oligomers and polymers: a molecular picture, Chem. Rev. 104 (2004) 4971–5003, doi:10.1021/cr040084k.
[43] B.H. Besler, K.M. Merz, P.A. Kollman, Atomic charges derived from semiempirical methods, J. Comput. Chem. 11 (1990) 431–439, doi:10.1002/jcc.540110404.
[44] J. Warnan, A. El Labban, C. Cabanetos, E.T. Hoke, P.K. Shukla, C. Risko, J.L. Br??das, M.D. McGehee, P.M. Beaujuge, Ring substituents mediate the morphology of PBDTTPD-PCBM bulk-heterojunction solar cells, Chem. Mater. 26 (2014) 2299–2306, doi:10.1021/cm500172w.
[45] B.A. DaSilveira Neto, A.S.A. Lopes, G. Ebeling, R.S. Gonçalves, V.E.U. Costa, F.H. Quina, J. Dupont, Photophysical and electrochemical properties of π-extended molecular 2,1,3-benzothiadiazoles, Tetrahedron 61 (2005) 10975–10982, doi:10.1016/j.tet.2005.08.093.
[46] C.Y. Kuo, Y.C. Huang, C.Y. Hsiow, Y.W. Yang, C.I. Huang, S.P. Rwei, H.L. Wang, L. Wang, Effect of side-chain architecture on the optical and crystalline properties of two-dimensional polythiophenes, Macromol. 46 (2013) 5985–5997, doi:10.1021/ma4007945.
[47] Q. Hou, Q. Zhou, Y. Zhang, W. Yang, R. Yang, Y. Cao, Synthesis and electroluminescent properties of high-efficiency saturated red emitter based on copolymers from fluorene and 4,7-Di(4-hexylthien-2-yl)-2,1, 3-benzothiadiazole, Macromol 37 (2004) 6299–6305, doi:10.1021/ma049204g.
[48] J. Kim, M.H. Yun, G.H. Kim, J. Lee, S.M. Lee, S.J. Ko, Y. Kim, G.K. Dutta, M. Moon, S.Y. Park, D.S. Kim, J.Y. Kim, C. Yang, Synthesis of PCDTBT-based fluorinated polymers for high open-circuit voltage in organic photovoltaics: towards an understanding of relationships between polymer energy levels engineering and ideal morphology control, ACS Appl. Mater. Interfaces. 6 (2014) 7523–7534, doi:10.1021/am500891z.
[49] H. Medlej, A. Nourdine, H. Awada, M. Abbas, C. Dagron-Lartigau, G. Wantz, L. Flandin, Fluorinated benzothiadiazole-based low band gap copolymers to enhance open-circuit voltage and efficiency of polymer solar cells, Eur. Polym. J. 59 (2014) 25–35, doi:10.1016/j.eurpolymj.2014.07.006.
[50] C. Gu, M. Xiao, X. Bao, L. Han, D. Zhu, N. Wang, S. Wen, W. Zhu, R. Yang, Design, synthesis and photovoltaic properties of two π-bridged cyclopentadithiophene-based polymers, Polym. Chem. 5 (2014) 6551–6557, doi:10.1039/c4py00881b.
[51] H. Hwang, Y. Kim, M. Kang, M.H. Lee, Y.J. Heo, D.Y. Kim, A conjugated polymer with high planarity and extended π-electron delocalization: via a quinoid structure prepared by short synthetic steps, Polym. Chem. 8 (2017) 361–365, doi:10.1039/c6py01729k.
[52] S.M. Risser, D.N. Beratan, S.R. Marder, Structure-Function Relationships for Beta, the First Molecular Hyperpolarizability, J. Am. Chem. Soc. 115 (1993) 7719–7728.
[53] X.P. Xu, Y. Li, M.M. Luo, Q. Peng, Recent progress towards fluorinated copolymers for efficient photovoltaic applications, Chinese Chem. Lett. 27 (2016) 1241–1249, doi:10.1016/j.cclet.2016.05.006.
[54] S.K. Putri, Y.H. Kim, D.R. Whang, M.S. Lee, J.H. Kim, D.W. Chang, Step-by-step improvement in photovoltaic properties of fluorinated quinoxaline-based low-band-gap polymers, Org. Electron. 47 (2017) 14–23, doi:10.1016/j.orgel.2017.04.025.
[55] N. Leclerc, P. Chávez, O.A. Ibraikulov, T. Heiser, P. Lévêque, Impact of backbone fluorination on π-conjugated polymers in organic photovoltaic devices: A review, Polymers (Basel) 8 (2016), doi:10.3390/polym8010011.
[56] D. Liu, W. Zhao, S. Zhang, L. Ye, Z. Zheng, Y. Cui, Y. Chen, J. Hou, Highly efficient photovoltaic polymers based on benzodithiophene and quinoxaline with deeper HOMO levels, Macromol 48 (2015) 5172–5178, doi:10.1021/acs.macromol.5b00829.
[57] L. Yang, J.R. Tumbleston, H. Zhou, H. Ade, W. You, Disentangling the impact of side chains and fluorine substituents of conjugated donor polymers on the performance of photovoltaic blends, Energy Environ. Sci. 6 (2013) 316–326, doi:10.1039/c2ee23235a.
[58] M. Zhang, X. Guo, S. Zhang, J. Hou, Synergistic effect of fluorination on molecular energy level modulation in highly efficient photovoltaic polymers, Adv. Mater. 26 (2014) 1118–1123, doi:10.1002/adma.201304427.
[59] T. Okamoto, K. Nakahara, A. Saeki, S. Seki, J.H. Oh, H.B. Akkerman, Z. Bao, Y. Matsuo, Aryl-perfluoroaryl substituted tetracene: Induction of face-to-face π-π Stacking and enhancement of charge carrier properties, Chem. Mater. 23 (2011) 1646–1649, doi:10.1021/cm200356y.
[60] K. Reichenbächer, H.I. Süss, J. Hulliger, Fluorine in crystal engineering—"the little atom that could, Chem. Soc. Rev. 34 (2005) 22–30, doi:10.1039/b406892k.
[61] L. Wang, S. Zhao, Z. Xu, J. Zhao, D. Huang, L. Zhao, Integrated effects of two additives on the enhanced performance of PTB7:PC71BM polymer solar cells, Materials (Basel) 9 (2016) 1–9, doi:10.3390/ma9030171.
[62] F. Meyer, Progress in polymer science fluorinated conjugated polymers in organic bulk heterojunction photovoltaic solar cells, Prog. Polym. Sci. 47 (2015) 70–91, doi:10.1016/j.progpolymsci.2015.04.007.
[63] I.C. Ghosekar, G.C. Patil, Review on performance analysis of P3HT:PCBM-based bulk heterojunction organic solar cells, Semicond. Sci. Technol. 36 (2021) 15, doi:10.1088/1361-6641/abe21b.
[64] J. Gao, R. Ming, Q. An, X. Ma, M. Zhang, J. Miao, J. Wang, C. Yang, F. Zhang, Ternary organic solar cells with J71 as donor and alloyed acceptors exhibiting 13.16% efficiency, Nano Energy 63 (2019) 103888, doi:10.1016/j.nanoen.2019.103888.
[65] Q.V. Hoang, C.E. Song, S.J. Moon, S.K. Lee, J.C. Lee, B.J. Kim, W.S. Shin, Asymmetric electron-donating 4-Alkyl-8-alkoxybenzo[1,2- b:4,5- b ′]dithiophene unit for use in high-efficiency bulk heterojunction polymer solar cells, Macromol. 48 (2015) 3918–3927, doi:10.1021/acs.macromol.5b00684.
[66] K.D. Deshmukh, R. Matsidik, S.K.K. Prasad, L.A. Connal, A.C.Y. Liu, E. Gann, L. Thomsen, J.M. Hodgkiss, M. Sommer, C.R. McNeill, Tuning the molecular weight of the electron accepting polymer in all-polymer solar cells: impact on morphology and charge generation, Adv. Funct. Mater. 28 (2018) 1707185, doi:10.1002/adfm.201707185.
[67] D.K. Tran, A. Robitaille, I.J. Hai, X. Ding, D. Kuzuhara, T. Koganezawa, Y.C. Chiu, M. Leclerc, S.A. Jenekhe, Elucidating the impact of molecular weight on morphology, charge transport, photophysics and performance of all-polymer solar cells, J. Mater. Chem. A. 8 (2020) 21070–21083, doi:10.1039/d0ta08195g.
[68] Z. Xiao, K. Sun, J. Subbiah, T. Qin, S. Lu, B. Purushothaman, D.J. Jones, A.B. Holmes, W.W.H. Wong, Effect of molecular weight on the properties and organic solar cell device performance of a donor-acceptor conjugated polymer, Polym. Chem. 6 (2015) 2312–2318, doi:10.1039/c4py01631a.
[69] X. Guo, M. Zhang, W. Ma, S. Zhang, J. Hou, Y. Li, Effect of solvent additive on active layer morphologies and photovoltaic performance of polymer solar cells based on PBDTTT-C-T /PC71BM, RSC Adv 6 (2016) 51924–51931, doi:10.1039/c6ra06020j.
[70] J.H. Kim, J.B. Park, H.U. Kim, I.N. Kang, D.H. Hwang, High open-circuit voltage organic photovoltaic cells fabricated using semiconducting copolymers consisting of bithiophene and fluorinated quinoxaline or triazole derivatives, Synth. Met. 194 (2014) 88–96, doi:10.1016/j.synthmet.2014.04.033.
[71] L. Feng, J. Yuan, Z. Zhang, H. Peng, Z.G. Zhang, S. Xu, Y. Liu, Y. Li, Y. Zou, Thieno[3,2-b]pyrrolo-fused pentacyclic benzotriazole-based acceptor for efficient organic photovoltaics, ACS Appl. Mater. Interfaces. 9 (2017) 31985–31992, doi:10.1021/acsami.7b10995.
[72] Q. Sun, F. Zhang, J. Wang, Q. An, C. Zhao, L. Li, F. Teng, B. Hu, A two-step strategy to clarify the roles of a solution processed PFN interfacial layer in highly efficient polymer solar cells, J. Mater. Chem. A. 3 (2015) 18432–18441, doi:10.1039/c5ta05117g.